DALTON
FULL PAPER

A theoretical study of $[M(PH_3)_4]$ (M = Ru or Fe), models for the highly reactive d^8 intermediates $[M(dmpe)_2]$ (dmpe = $Me_2PCH_2CH_2PMe_2$). Zero activation energies for addition of CO and oxidative addition of H_2 ‡

Stuart A. Macgregor,*,†,[a] Odile Eisenstein,[a] Michael K. Whittlesey[b] and Robin N. Perutz[b]

[a] *Laboratoire de Chimie Théorique, Bâtiment 490, Université de Paris-Sud, 91405 Orsay, France*
[b] *Department of Chemistry, University of York, York, UK YO1 5DD*

Density functional calculations have been carried out on $[M(PH_3)_4]$ species as models for transient $[M(dmpe)_2]$ formed from the photolysis of $[M(dmpe)_2H_2]$ (M = Ru or Fe, dmpe = $Me_2PCH_2CH_2PMe_2$). Calculations have also been performed on $[Rh(PH_3)_4]^+$ as a model for the relatively inert $[Rh(dmpe)_2]^+$. The singlet electron configurations of $[Ru(PH_3)_4]$ and $[Rh(PH_3)_4]^+$ were found to have D_{2d} geometries with *trans* P–M–P angles of 159 (M = Ru) and 172° (M = Rh^+). Singlet $[Fe(PH_3)_4]$ was computed to have a C_{2v} structure with *trans* P–M–P angles of 137 and 160° at Fe. The triplet configurations of $[Fe(PH_3)_4]$ and $[Ru(PH_3)_4]$ were predicted to adopt C_{2v} geometries with angles of *ca.* 155 and 95° for both species. Singlet $[Ru(PH_3)_4]$ is calculated to be 11.7 kcal mol^{-1} more stable than the triplet, but the triplet form of $[Fe(PH_3)_4]$ is the more stable by 8.0 kcal mol^{-1}. The addition of CO and oxidative addition of H_2 to $[M(PH_3)_4]$ (M = Ru or Fe) were calculated to be highly exothermic. In contrast, the reaction between $[Rh(PH_3)_4]^+$ and H_2 is less thermodynamically favoured, consistent with the lower reactivity of experimental Rh^+ analogues. Both the oxidative addition of H_2 and addition of CO were calculated to proceed without activation energy for $[Ru(PH_3)_4]$, but only once the 'end-on' approach of H_2 and an angled approach of CO at long ruthenium–substrate separations are considered. The calculations on $[Ru(PH_3)_4]$ also reproduced the UV/VIS spectrum and geometry of $[Ru(dmpe)_2]$ satisfactorily. The reaction of singlet $[Fe(PH_3)_4]$ with CO was calculated to be barrierless, while the oxidative addition of H_2 required a very small activation energy (≈1 kcal mol^{-1}) at long Fe–H_2 distances. The reaction of $[Rh(PH_3)_4]^+$ with H_2 has a somewhat larger activation barrier (≈3 kcal mol^{-1}) and is predicted to pass through a product-like C_{2v} transition state.

The problem of the geometry and reactivity of d^8 ML_4 complexes is longstanding and complex. Geometries close to tetrahedral with triplet spin states are found for first-row transition metals of Groups 9 and 10, while square-planar geometries with singlet spin states are common for second- and third-row metals of the same groups. The ML_4 complexes of Group 8 metals are highly reactive molecules which have only a transient existence under conventional conditions. The importance of such molecules lies in their ability to undergo a large number of reactions, including co-ordination of an additional ligand, oxidative addition with reagents such as dihydrogen, and formation of metal–metal bonds. The isolobal analogy between d^8 ML_4 and carbenes[1] highlights the problem of spin state and geometry as well as the high reactivity of these molecules.

The first such molecule to be studied in detail was $[Fe(CO)_4]$.[2] Matrix infrared and gas-phase time-resolved infrared (TRIR) experiments showed that this molecule adopts a C_{2v} structure with C–Fe–C angles of 147 and 120° and two unpaired electrons. As a result of a triplet ground state, the rate constants for its reaction with CO and H_2 in the gas phase are 2–3 orders of magnitude lower than for the corresponding reactions of $[Cr(CO)_5]$.[3] When xenon or methane matrices are used in place of argon, triplet $[Fe(CO)_4]$ is replaced by a species identified as $[Fe(CO)_4S]$ (S = Xe or CH_4) which has a trigonal-bipyramidal structure with S in the equatorial plane. The C–Fe–C angles are now 174 and 125°; it is thought that the electrons are spin-paired.[2] Far less is known about the nature of $[Fe(CO)_4]$ as a transient species in solution. A recent summary of experimental results, collated by Grevels,[4] indicates that the first species to be observed after laser flash photolysis of $[Fe(CO)_5]$ in cyclohexane is $[Fe(CO)_4(C_6H_{12})]$, *i.e.* the analogue of $[Fe(CO)_4S]$, which is formed within the instrumental risetime of 3 μs. Any triplet $[Fe(CO)_4]$ must have a much shorter lifetime in solution. Thus the results indicate that three ML_4 species need to be considered: a triplet, a singlet and a solvent adduct, ML_4S. The structures of the triplet and singlet may both be far from the tetrahedral and square-planar limits.

The ruthenium analogue, $[Ru(CO)_4]$, has been studied by TRIR in the gas phase, but the spectral data do not permit the structure to be determined. However, the high rate constant for reaction with CO indicates that $[Ru(CO)_4]$ has a singlet ground state.[5]

The combination of matrix isolation and time-resolved absorption spectroscopy in solution has recently been applied with considerable success to ML_4-type complexes with chelating phosphine ligands, $[M(dmpe)_2]$ (M = Fe or Ru, dmpe = $Me_2PCH_2CH_2PMe_2$).[6,7] These complexes are usually generated by photolysis of the corresponding dihydrides, $[M(dmpe)_2H_2]$. The ruthenium complex, $[Ru(dmpe)_2]$, shows a three-band UV/VIS spectrum and reacts with both H_2 and CO at rates close to the diffusion limit (>1 × 10^9 dm^3 mol^{-1} s^{-1}). The spectrum suggests that it adopts a geometry very close to square planar. The large rate constants indicate that there is no barrier to reaction created by spin-state interconversion, and hence that $[Ru(dmpe)_2]$ has a singlet ground state. The NMR evidence demonstrates that $[Ru(dmpe)_2]$ undergoes oxidative-addition reactions with benzene, but not with alkanes.[8]

Recently, $[Ru(CO)_2L_2]$ (L = PBu^t_2Me) was isolated in a singlet ground state and shown by X-ray crystallography to have a C_{2v} structure with C–Ru–C 133.3° and P–Ru–P 165.6°.

† *Present Address*: Department of Chemistry, Heriot-Watt University, Riccarton, Edinburgh, UK EH14 4AS.

‡ *Supplementary data available*: calculated coordinates and energies. For direct electronic access see http://www.rsc.org/suppdata/dt/1998/291/, otherwise available from BLDSC (No. SUP 57317, 12 pp.) or the RSC Library. See Instructions for Authors, 1998, Issue 1 (http.//www.rsc.org/dalton). *Non-SI unit employed*: cal = 4.184 J.

Like the other d^8 RuL_4 complexes, it reacts very rapidly with several molecules.[9] The analogue with $L = PMe_3$ has been studied in low-temperature matrices and shown to have C–Ru–C larger than 130° and to form adducts of the type $[Ru(CO)_2(PMe_3)_2S]$ (S = Xe or CH_4).[10] *Ab initio* second-order Møller-Plesset perturbation (MP2) calculations on $[Ru(CO)_2(PH_3)_2]$ have revealed a C_{2v} structure, indicating that the C–Ru–C bond angle is not constrained either by steric effects or the presence of S.[9]

The iron complex $[Fe(dmpe)_2]$,[6] exhibits very different characteristics from its ruthenium analogue. The lowest-energy absorption is in the near-UV region at *ca.* 28 000 cm^{-1}, the rate constant for reaction with H_2 is a factor of 7500 smaller than for $[Ru(dmpe)_2]$, whereas the rate constant for reaction with CO is only a factor of two slower. Oxidative-addition reactions with arenes and with alkanes compete effectively with the back reaction with H_2. The NMR investigations provide decisive evidence that even methane reacts with $[Fe(dmpe)_2]$.[11] Thus $[Fe(dmpe)_2]$ is substantially less reactive than $[Ru(dmpe)_2]$ towards H_2, but more reactive towards hydrocarbons. The differences in spectra and reactivity between $[Fe(dmpe)_2]$ and $[Ru(dmpe)_2]$ suggest that $[Fe(dmpe)_2]$ is not square planar. Although the high rate constant for reaction with CO makes a singlet ground state for $[Fe(dmpe)_2]$ likely, it is not close enough to the diffusion limit to be decisive. The experimental data show that any effect of specific complexation by the solvent on the kinetics of reaction of $[Fe(dmpe)_2]$ is very slight.

The structures of d^8 ML_4 species have also been investigated extensively by theoretical methods. Burdett[12] predicted on the basis of extended Hückel calculations that high-spin d^8 $[M(CO)_4]$ complexes should adopt a C_{2v} structure with angles of 110 and 135°. He noted that the square-planar geometry was preferred for low-spin d^8, but that a D_{2d} distortion was preferred over a C_{3v} distortion. The conclusions from Burdett's angular overlap analysis paralleled those from the extended Hückel calculations.[13] Since the angular overlap arguments were based solely on σ interactions, they should be applicable (in a first approximation) to metal phosphine as well as metal carbonyl complexes. Elian and Hoffmann,[14] who included the metal–ligand d_π/p_π interactions in their calculations, predicted a D_{2d} geometry (angle *ca.* 150°) for a d^8 low-spin $[M(CO)_4]$ molecule, but a square-planar geometry for the corresponding MCl_4 complex. They did not consider the high-spin case. Ziegler and co-workers[15] returned to these problems with density functional calculations. This work predicts that $[Fe(CO)_4]$ and $[Ru(CO)_4]$ would have C_{2v} structures both in their singlet and in their triplet states, that the angles in the singlet states should be *ca.* 175 and 130°, and that the angles in the triplet states should be *ca.* 155 and 95°. The singlet state was strongly favoured for $[Ru(CO)_4]$, but the two states were almost equienergetic for $[Fe(CO)_4]$. Ziegler *et al.*[15a] also examined the pathways for reaction of $[Ru(CO)_4]$ with H_2 and CH_4. Notable features were: (i) formation of σ complexes as reaction intermediates albeit with very shallow potential wells, (ii) oxidative addition of H_2 with an activation energy of *ca.* 2.6 kcal mol^{-1} and (iii) oxidative addition of methane with a barrier of 19 kcal mol^{-1}. Wang and Weitz[16a] have re-examined both singlet and triplet $[Fe(CO)_4]$ and published a critique of the various estimates of the singlet–triplet energy separation.

Many other theoretical studies of the addition of small molecules to unsaturated transition-metal species have been performed at various levels of theory.[17–27] These calculations have repeatedly demonstrated the existence of potential minima for σ complexes of H_2 and CH_4 prior to full oxidative addition. The importance of σ complexes is supported by a large body of experimental evidence.[28]

We report a theoretical study designed to reveal the molecular structure and ground electronic configuration of $[Fe(dmpe)_2]$ and $[Ru(dmpe)_2]$ and to examine the pathways for co-ordination of CO and oxidative addition of H_2 to these molecules. We have employed $[M(PH_3)_4]$ (M = Ru or Fe) as model compounds and used density functional methods[29] which have proved to be particularly effective in reproducing the molecular geometries, dissociation energies and reactivity trends of transition-metal systems.[30]

The present study also includes a number of calculations on the isoelectronic model system $[Rh(PH_3)_4]^+$. Many tetrakis(phosphine)rhodium(I) species are known experimentally and several have been characterised crystallographically, including $[Rh(dmpe)_2]^+$.[31,32] In the absence of structural information on the ruthenium and iron systems, this provides us with an experimental standard against which we can compare our computed results. In addition, whereas $[Fe(dmpe)_2]$ and $[Ru(dmpe)_2]$ are both extremely reactive species, their rhodium(I) analogue is relatively unreactive. We should therefore expect our computed results to reflect this large difference in reactivity before we can tackle the subtler distinctions between the ruthenium and iron systems with confidence. Jones *et al.*[32] reported that $[Rh(PMe_3)_4]^+$ undergoes oxidative addition with H_2. The reactivity of $[Rh(PR_2R')_4]^+$ with H_2 has been studied by Schrock and Osborn.[33] They found when R = Me and R′ = Ph that oxidative addition occurred with the formation of $[Rh(PMe_2Ph)_4H_2]^+$. However, when R = Ph and R′ = Me or R = OMe and R′ = Ph no reaction was observed. Clearly the reactivity of these rhodium(I) systems is very sensitive to the steric and electronic properties of the phosphine. In the following we use the oxidative addition of H_2 to $[M(PH_3)_4]$ (M = Ru, Fe or Rh^+) as a test of our computational approach.

Computational Details

All calculations used the Amsterdam Density Functional program (ADF, version 2.0.1) developed by Baerends *et al.*[34] and employed the numerical integration scheme of te Velde and Baerends.[35] For Ru, Fe and Rh a triple-ζ-STO (Slater type orbital) basis set was employed. For P, O, C and PH_3 hydrogen atoms a double-ζ-STO basis set extended by a polarisation function was used. All hydrogen atoms directly involved in bonding to a metal were described using a triple-ζ-STO basis set extended with two polarisation functions. An auxiliary set of s, p, d, f and g STO basis functions centred on all nuclei was used in order to fit the molecular density and describe accurately the Coulomb and exchange potentials in each SCF (self-consistent field) cycle.[36] Core electrons (up to and including 3d for Ru and Rh, 2p for Fe and P and 1s for C and O) were treated using the frozen-core approximation.[34] The calculations incorporated the quasi-relativistic corrections of Ziegler *et al.*[37] Geometry optimisation was carried out using the local density approximation (LDA) employing the parameterisation of Vosko *et al.*[38] and made use of the optimisation procedure developed by Versluis and Ziegler.[39] Geometries were fully optimised under the appropriate symmetry constraints. Test calculations on the C_{2v} geometries of singlet and triplet $[M(PH_3)_4]$ species (M = Fe or Ru) in which symmetry constraints were relaxed first to C_s and then C_1 symmetry gave very similar results. Energies of all optimised structures were recalculated with the BP86 functional, including the non-local (NL) corrections of Becke[40] (exchange) and Perdew[41] (correlation). Electronic transition energies and ionisation potentials were calculated using the ΔSCF method. Total computed energies (at both local and non-local levels of calculation) and cartesian coordinates for all optimised structures are available as supplementary information (SUP 57317).

Results

Structures of $M(PH_3)_4$ species

Singlet electronic configuration (M = Ru, Fe or Rh^+). The geometries of $[M(PH_3)_4]$ (M = Ru, Fe or Rh^+) were optimised

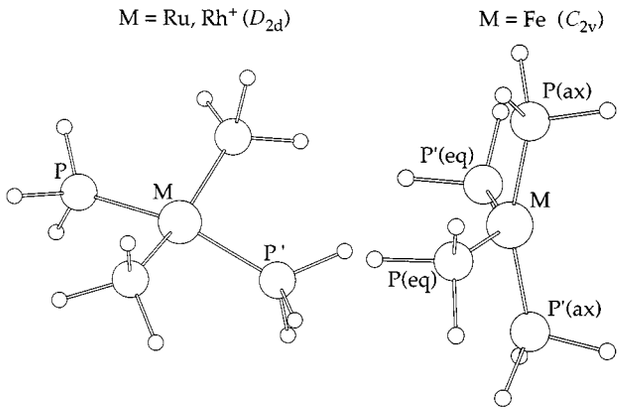

	M = Ru	M = Rh+	M = Fe	
M-P	2.239	2.239	M-P(eq)	2.088
P′-M-P	158.6	172.2	M-P(ax)	2.103
			P(eq)-Fe-P′(eq)	137.0
			P(ax)-Fe-P′(ax)	159.7

Fig. 1 Geometries (distances in Å, angles in °) of singlet $[M(PH_3)_4]$ species (M = Fe, Ru or Rh^+)

for a singlet electronic configuration under the C_{2v} symmetry constraint, corresponding to a staggered arrangement of the PH_3 ligands. The optimised structures of all three species exhibit distortions away from a square-planar geometry (see Fig. 1). For $[Ru(PH_3)_4]$ and $[Rh(PH_3)_4]^+$ the MP_4 cores are close to overall D_{2d} symmetry with the M–P bonds being displaced away from a square-planar geometry by an average of 10.7 (M = Ru) and 3.9° (M = Rh^+). For $[Fe(PH_3)_4]$ we calculate a C_{2v} structure with angles of 137.0 and 159.7° at the metal.

The calculated average M–P bond length for $[Rh(PH_3)_4]^+$ is 2.239 Å. This is somewhat shorter than the distance found experimentally in the crystal structure of $[Rh(dmpe)_2]^+$ (Rh-P 2.282 Å) in which the geometry at the metal is very close to square planar.[31] In the crystal structure of $[Rh(PMe_3)_4]^+$ the *trans* P–Rh–P angles average 150°; this larger distortion is probably due to steric crowding of the phosphine ligands.[32] The Rh–P distances in this species average 2.297 Å. Comparison of the two experimental structures suggests that one effect of the chelating phosphine may be to force the geometry nearer to square planar. Thus, in the case of $[Ru(PH_3)_4]$ the deviation away from square-planar geometry may be a consequence of the inability of PH_3 to model fully the dmpe ligand, especially its steric bulk and the consequences of its bidentate binding mode. The calculated average Ru–P distance in this species (2.239 Å) is again shorter than those found experimentally in related species, for example $[Ru(dmpe)_2(CO)]$, in which the Ru–P distances average 2.297 Å.[42] The underestimation of metal–ligand bond lengths is usually found when the LDA (local density approximation) level of theory is employed.[30]§ Optimising $[Ru(PH_3)_4]$ in C_{2v} symmetry but constraining the RuP_4 core to a square-planar geometry yielded an average Ru–P bond distance of 2.246 Å and a calculated energy only 2 kcal mol^{-1} higher than the global D_{2d} minimum. As has been suggested previously,[14] the deformation of the d^8 MP_4 core appears relatively facile.

The calculated C_{2v} structure of $[Fe(PH_3)_4]$ has Fe–P bonds of 2.103 (axial) and 2.088 Å (equatorial). These calculated distances are somewhat shorter than expected, even given the usual underestimation of metal–ligand bonds with the LDA. A review of structures contained in the Cambridge Structural Database gave Fe–PR_3 distances of 2.246 (R = Me, average of 20 systems) and 2.237 Å (R = Ph, average of 31 systems).[43] The

§ Reoptimisation of $[Ru(PH_3)_4]$ including non-local gradient corrections yielded an equivalent (to within 0.5°) D_{2d} structure with an average Ru–P bond length of 2.268 Å.

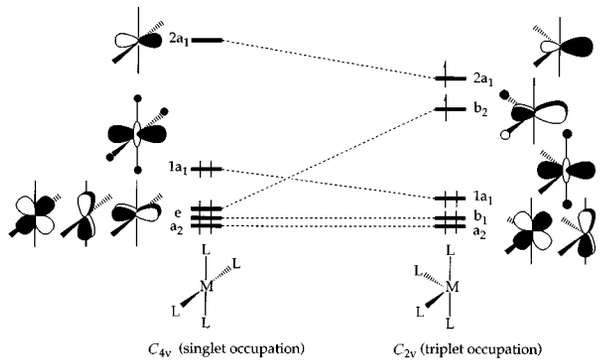

Fig. 2 Schematic representation of ML_4 valence orbital changes upon C_{4v} to C_{2v} distortion

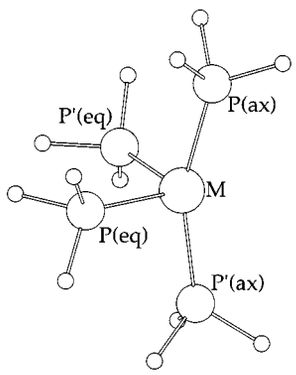

	M = Fe	M = Ru
M-P(eq)	2.130	2.279
M-P(ax)	2.160	2.229
P(eq)-M-P′(eq)	95.8	94.0
P(ax)-M-P′(ax)	154.0	158.5

Fig. 3 Geometries of triplet $[M(PH_3)_4]$ species (M = Fe or Ru)

short calculated Fe–P distances may arise from the lack of steric crowding around the small iron metal centre in our model compounds.

Triplet electronic configuration (M = Ru or Fe). Optimisations for the triplet structures of $[M(PH_3)_4]$ species (M = Ru or Fe) were based upon a bent C_{2v} structure. The deformation of square-planar d^8 ML_4 species towards such a structure is known to lead to a reduction in the HOMO–LUMO (highest occupied–lowest unoccupied molecular orbital) gap.[44] A formally nonbonding (neglecting π effects) metal-based d orbital is strongly destabilised while, at the same time, an unoccupied metal p orbital is stabilised (see Fig. 2).

Geometries for the triplet electronic configuration were therefore optimised for single occupation of the appropriate b_2 and a_1 orbitals (Fig. 2, right-hand side) under the C_{2v} symmetry constraint. The geometries obtained (see Fig. 3) are similar to those of the triplet forms of $[M(CO)_4]$ (M = Fe or Ru) calculated by Ziegler and co-workers[3] and that obtained more recently by Wang and Weitz[16a] for $[Fe(CO)_4]$. Using an equivalent method to that used here, both sets of authors calculated triplet $[Fe(CO)_4]$ to be slightly more stable (< 2 kcal mol^{-1}) than the singlet,¶ in accord with the experimental evidence that 'naked' $[Fe(CO)_4]$ exists as a triplet.[2,3] The singlet form of $[Ru(CO)_4]$ was calculated to be significantly more stable than

¶ It has been pointed out that calculated singlet–triplet separations can be dependent on the density functional employed and that the B3LYP functional exhibits a greater preference for the higher spin-state species than does the BP86 functional used here.[16a] Recently, Ruiz *et al.*[16b] have found the B3LYP functional to be especially effective at reproducing the singlet–triplet energy difference in hydroxy- and alkoxo-bridged copper(II) binuclear complexes.

the triplet.[15] For $[Ru(PH_3)_4]$ the singlet is more stable by 11.7 kcal mol^{-1}, but for $[Fe(PH_3)_4]$ the triplet was more stable than the singlet by 8.0 kcal mol^{-1}. The singlet–triplet energy gap is therefore significantly larger for $[Fe(PH_3)_4]$ than for $[Fe(CO)_4]$.

UV/VIS spectra. The experimental evidence for the structure of $[Ru(dmpe)_2]$ is based mainly on its UV/VIS spectrum which exhibits three low-energy absorption bands and is consistent with a square-planar geometry. The lowest-energy band is assigned as a $d_{z^2} > p_z$ transition on the basis of its absorption coefficient and occurs experimentally at 13 800 cm^{-1} in pentane solution. The equivalent transition occurs at 25 600 cm^{-1} for square-planar $[Rh(dmpe)_2]^+$ in methanol.[7] The calculated energies of these transitions in the $[M(PH_3)_4]$ model species are 13 900 and 26 200 cm^{-1} for M = Ru and Rh^+ respectively. Thus, we find remarkably good reproduction of the experimental trend.

For $[Fe(dmpe)_2]$ in pentane solution a single band has been observed at 28 200 cm^{-1}.[6] The $d_{z^2} > p_z$ transition in singlet $[Fe(PH_3)_4]$ is calculated to occur at 2530 cm^{-1}, and so the lowest-energy excitation would be expected to occur in the IR region of the spectrum. However, as we have seen, the dmpe ligand appears to favour a planar structure. Recalculation of this transition energy for square-planar $[Fe(PH_3)_4]$ [optimised under C_{2v} symmetry, Fe-P (average) = 2.107 Å] gives a value of 6600 cm^{-1}. This suggests a low-lying band would be seen in the visible/near-IR spectrum of square-planar singlet $[Fe(dmpe)_2]$. Following this prediction, we measured the spectrum of $[Fe(dmpe)_2]$ in an argon matrix from 4000 to 12 500 cm^{-1}, a region which has not been examined previously. No absorptions were detected.

In summary, our calculations on $[Ru(PH_3)_4]$ support the experimental evidence that $[Ru(dmpe)_2]$ has a singlet electronic configuration in the ground state and a structure close to square planar. For $[Fe(PH_3)_4]$ the calculations favour the triplet structure. The experimental data on $[Fe(dmpe)_2]$ do not provide direct evidence for or against a triplet state, nor do they preclude a spin-state equilibrium.

Reactivity of $[M(PH_3)_4]$ species with H_2 and CO

The reactivity of $[M(dmpe)_2]$ species was modelled by computing the reaction profiles for the approach of the substrate molecules towards the $[M(PH_3)_4]$ model species in the singlet electronic configuration. The energy of each point on the reaction profile was then plotted relative to that of the reactants in their optimum singlet-state geometries. We do not include any correction for zero-point energies. The difference in zero-point energy between products and reactants for the oxidative addition of H_2 is estimated to be about 2.2 kcal mol^{-1} based on two M–H stretching frequencies at 1770 cm^{-1} and four deformations modes at 600 cm^{-1}.

Oxidative addition of H_2 to $[M(PH_3)_4]$ (M = Ru, Fe or Rh^+). The geometries of the octahedral products of oxidative addition of H_2 to $[M(PH_3)_4]$ are shown in Fig. 4 along with the calculated energies of formation (ΔE^{form}) for the products. As expected, the two (equatorial) phosphine ligands in the plane of addition bend away from the hydride ligands while the other two (axial) phosphines incline slightly towards the H···H midpoint. The optimised M–H bond lengths compare well with available neutron diffraction data: in $[Fe(dppe)_2H(H_2)]^+$ the Fe–H bond is 1.535 Å[45] and the Fe–H distance averages 1.526 Å in $[Fe(PEtPh_2)_3H_2(H_2)]$[46] compared with a computed value of 1.511 Å. The Rh–H distance in $[Rh(\eta^5\text{-}C_5Me_5)H_2(SiEt_3)_2]$[47] average 1.581 Å compared with the calculated Rh–H value of 1.598 Å, while the computed Ru–H distance of 1.643 Å compares to experimental values of 1.630 Å in $[Ru(\eta^5\text{-}C_5H_5)(PMe_3)_2H]$ and 1.602 Å (average) in $[Ru(\eta^5\text{-}C_5H_5)(PMe_3)_2H_2]^+$.[48] In all three structures the *trans* influence of the hydride ligand

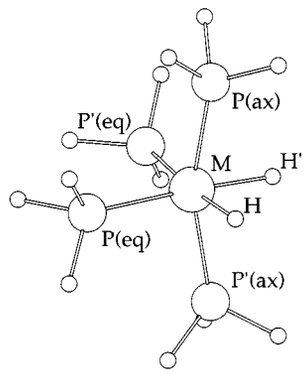

	M = Fe	M = Ru	M = Rh^+
M-H	1.511	1.643	1.598
M-P(eq)	2.123	2.281	2.295
M-P(ax)	2.100	2.252	2.249
H-M-H′	84.5	83.4	84.0
P(eq)-M-P′(eq)	99.6	98.2	99.0
P(ax)-M-P′(ax)	152.8	161.0	160.4
ΔE^{form}/kcal mol^{-1}	-42.6	-37.6	-15.6

Fig. 4 Geometries of singlet $[M(PH_3)_4H_2]$ species (M = Fe, Ru or Rh^+)

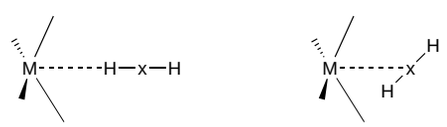

η^1 approach η^2 approach

Scheme 1

causes the equatorial M–P bonds to be slightly longer than both the M-P axial bonds and the M–P distances calculated for the four-co-ordinate singlet reactants. Little elongation of the axial M–P bonds is seen.

The large negative values obtained for ΔE^{form} with singlet $[Fe(PH_3)_4]$ and $[Ru(PH_3)_4]$ (−42.6 and −37.6 kcal mol^{-1} respectively) suggest a strong thermodynamic drive for the addition of H_2. With triplet $[Fe(PH_3)_4]$ ΔE^{form} is calculated to be −34.4 kcal mol^{-1}. For $[Rh(PH_3)_4]^+$ the thermodynamic driving force is much smaller (ΔE^{form} = −15.6 kcal mol^{-1}). The calculated values of ΔE^{form} are therefore consistent with the high reactivity of the experimental ruthenium and iron analogues and with the relatively lower reactivity of Rh^+ experimental analogues towards oxidative addition of H_2.

In order to understand the origin of the high reactivity of the neutral $[M(PH_3)_4]$ systems toward H_2, we have computed reaction profiles for the oxidative-addition process. Previous studies have found that an 'end-on' (or η^1) approach of H_2 is energetically favoured over a 'side-on' (or η^2) approach at long M–(H_2) separations.[18–20] Two reaction profiles corresponding to these two different orientations of the H_2 moiety relative to the $[M(PH_3)_4]$ reactant were therefore considered. Both were computed within C_{2v} symmetry and defined by the M–x distance, x being the H···H midpoint (Scheme 1). All other variables were optimised.

Profiles for the reaction of $[Ru(PH_3)_4] + H_2$ (Fig. 5) compare the η^1 and η^2 approaches calculated both at the LDA level and with the inclusion of non-local corrections, LDA + NL. At the LDA level the η^1 approach is indeed favoured at long Ru–x distances (>2.4 Å) and, within C_{2v} symmetry, a $[Ru(PH_3)_4(\eta^1\text{-}H_2)]$ adduct is formed with Ru–x 2.25 Å. This species is calculated to be 9.0 kcal mol^{-1} more stable than the isolated reactants. At shorter Ru–x distances the η^1 approach is rapidly destabilised. When the geometry of the C_{2v} adduct is reoptimised in C_s symmetry the H_2 moiety moves off the local C_2 axis

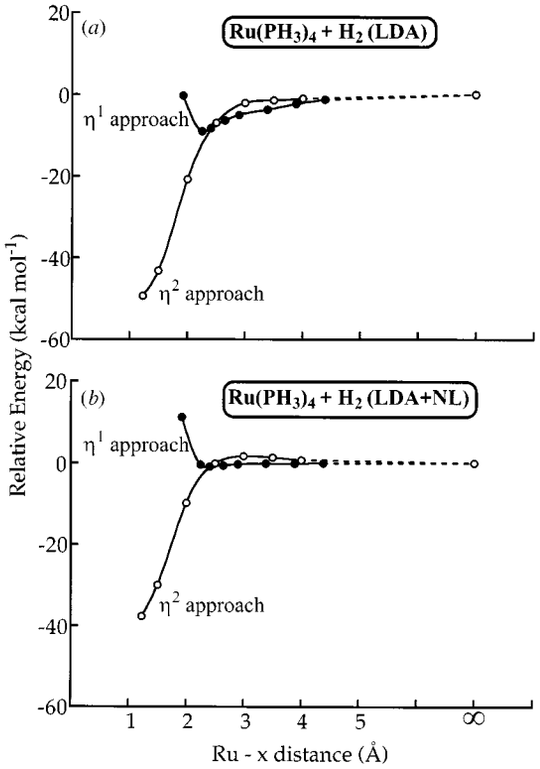

Fig. 5 Reaction profiles for the η^1 and η^2 approaches of H_2 towards singlet $[Ru(PH_3)_4]$ calculated at the LDA level (*a*) and including non-local corrections (LDA + NL) (*b*)

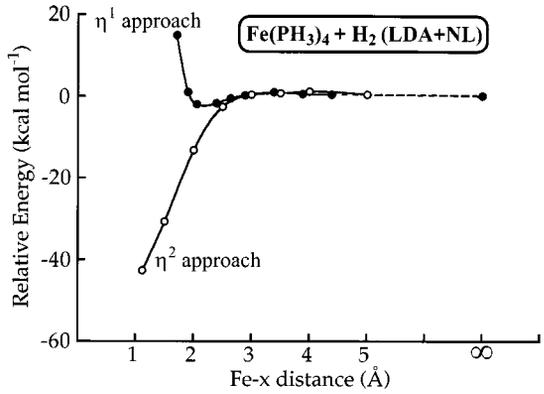

Fig. 6 Reaction profiles for the η^1 and η^2 approaches of H_2 towards singlet $[Fe(PH_3)_4]$ (LDA + NL)

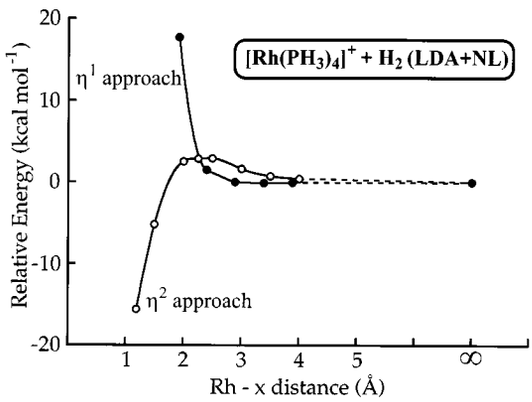

Fig. 7 Reaction profiles for the η^1 and η^2 approaches of H_2 towards singlet $[Rh(PH_3)_4]^+$ (LDA + NL)

and the optimised structure of the final $[Ru(PH_3)_4H_2]$ species is obtained. The addition of H_2 to $[Ru(PH_3)_4]$ *via* an η^2 approach is calculated to proceed without any activation barrier at the LDA level.

Similar trends are seen in the reaction profiles calculated at the LDA + NL level [Fig. 5(*b*)]. The η^1 approach remains favoured at long Ru–x distances and, within C_{2v} symmetry, a $[Ru(PH_3)_4(\eta^1\text{-}H_2)]$ adduct is formed without any activation barrier. This species is only 1 kcal mol^{-1} more stable than the isolated reactants. Significantly, at this level of calculation the η^2 approach of H_2 towards $[Ru(PH_3)_4]$ is computed to have a small activation barrier (≈ 2 kcal mol^{-1}). This result is inconsistent with the kinetic data for the oxidative addition of H_2 to $[Ru(dmpe)_2]$ which indicate the absence of an activation barrier for this reaction. As we have only included non-local corrections as a perturbation on the LDA results and not self-consistently in the computation of the reaction geometries, we cannot be certain that the $[Ru(PH_3)_4(\eta^1\text{-}H_2)]$ adduct corresponds to a local minimum at the LDA + NL level. Likewise, true transition states involved in these processes have not been optimised (as no transition state is calculated in the LDA reaction profiles) and so we only provide estimates of the energies associated with these species from the shape of the LDA + NL reaction profiles.

The reaction profiles calculated at the LDA level for the reactions of $[Fe(PH_3)_4]$ and $[Rh(PH_3)_4]^+$ with H_2 are similar to those described above for $[Ru(PH_3)_4]$. For $[Fe(PH_3)_4]$ at the LDA + NL level a small activation barrier (≈ 1 kcal mol^{-1}) is associated with both the η^1 and η^2 approaches of H_2 at Fe–x separations greater than 3 Å (Fig. 6). Within C_{2v} symmetry we compute the presence of an η^1 adduct with Fe–x 2.1 Å at this level. In contrast, for $[Rh(PH_3)_4]^+ + H_2$ (Fig. 7) no η^1 adduct is predicted: the LDA + NL curve for η^1 approach is weakly repulsive at long Rh–x distances and is destabilised above the η^2 approach at Rh–x ≈ 2.3 Å. An activation energy of approximately 3 kcal mol^{-1} is required for the η^2 approach of H_2 in this case and the transition state occurs with an Rh–x distance of approximately 2.3 Å. Note that at the LDA level the η^2 approach of H_2 towards $[Rh(PH_3)_4]^+$ is calculated to proceed without any activation barrier. This result is inconsistent with the relatively low reactivity of experimental rhodium(I) analogues and stresses the need to include non-local corrections in the computation of reaction profiles.

For all three systems therefore, the optimum reaction coordinate for addition of H_2 may involve an η^1 approach early in the reaction. As the M–x distance decreases further the H_2 fragment must swing round into an η^2 conformation. To investigate this process we have calculated a third reaction profile defined by the M–H–H angle, θ. The η^1 adducts described above have θ = 180°, while at the other extreme the final octahedral oxidative-addition products have θ ≈ 48°. Fig. 8 shows this reaction profile for $[Ru(PH_3)_4]$, computed at the LDA + NL level, as well as a schematic representation of the changes in *r*(H–H), *r*(Ru–H) and the P_{eq}–Ru–P_{eq} angle during the approach of H_2 toward $[Ru(PH_3)_4]$. Most significantly, the η^1/η^2 swing proceeds without activation energy for the $Ru(PH_3)_4 + H_2$ reaction. This contrasts with the reaction profile computed for the oxidative addition of H_2 to $[Ru(CO)_4]$ which displayed a distinct activation barrier.[15a] However, only the η^2 approach of H_2 was considered in that study, whereas the results presented here indicate that the orientation of the H_2 moiety during the oxidative-addition reaction can be important in determining activation barriers. Fig. 8 shows that the steep fall in energy begins when *r*(Ru–H) ≈ 1.77 Å and θ = 140°. At this stage P_{eq}–Ru–P_{eq} also starts to decline rapidly. However, the value of *r*(H–H) remains little changed until θ = 100° at which *r*(Ru–H) = 1.65 Å is close to its final value of 1.64 Å. Only then elongation of H–H occurs. Similar results were obtained with $[Fe(PH_3)_4]$. In contrast, for $[Rh(PH_3)_4]^+$ the η^1/η^2 swing requires an activation energy of >4 kcal mol^{-1}.

Addition of CO to $[M(PH_3)_4]$ (M = Ru or Fe). The addition reaction with CO was studied with $[Ru(PH_3)_4]$ and $[Fe(PH_3)_4]$.

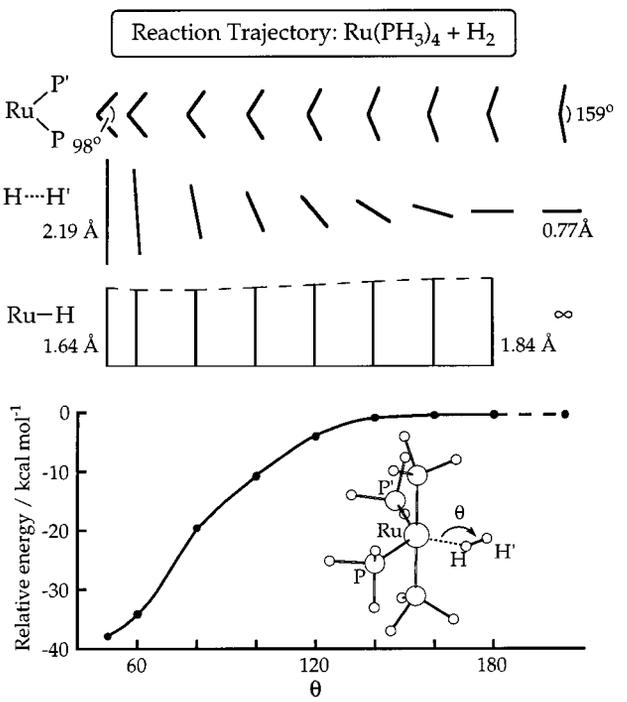

Fig. 8 Reaction profile and schematic representation of geometrical changes for the η^1/η^2 swing of H_2 with singlet $[Ru(PH_3)_4]$ (LDA + NL). Energies are relative to the sum of the isolated reactants set to zero, as indicated at the extreme right of the profile

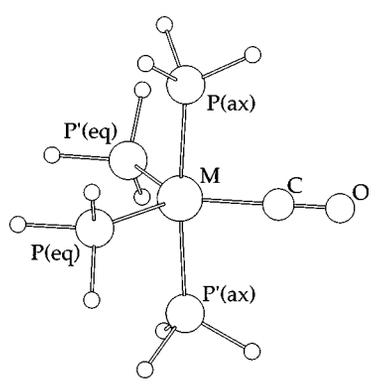

	M = Fe	M = Ru
M-C	1.714	1.870
C-O	1.169	1.167
M-P(eq)	2.134	2.288
M-P(ax)	2.131	2.272
P(eq)-M-P′(eq)	111.2	110.5
P(ax)-M-P′(ax)	174.8	173.2
ΔE^{form}/kcal mol^{-1}	-59.5	-43.5

Fig. 9 Geometries of $[M(PH_3)_4(CO)]$ species (M = Fe or Ru)

Since the experimental analogues of $[Rh(PH_3)_4]^+$ undergo phosphine substitution with CO rather than forming an addition product,[32] this system was not studied.

The geometries of the five-co-ordinate product species optimised in C_{2v} symmetry are shown in Fig. 9. As for the dihydride species, the equatorial M–P bonds are somewhat longer than the axial M–P bonds. The calculated Ru–C bond distance (1.870 Å) is comparable to that found experimentally for $[Ru(dmpe)_2(CO)]$ (1.850 Å).[42] The calculated Fe–C bond length (1.714 Å) is shorter than those found in the structure of $[Fe(dppm)(CO)_3]$ (dppm = $Ph_2PCH_2PPh_2$) in which the average Fe–C bond distance is 1.76 Å.[49] The energy of formation for the two products (−59.5 and −43.5 kcal mol^{-1} for M = Fe and Ru

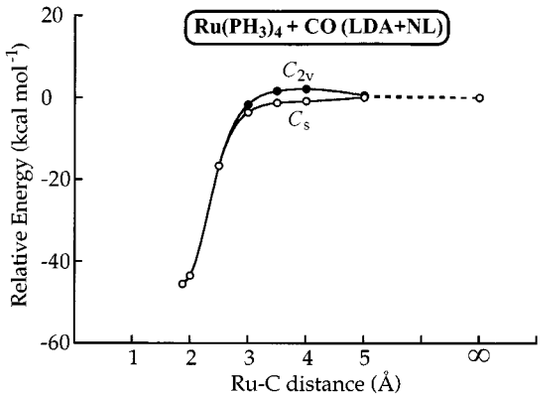

Fig. 10 Reaction profiles for the addition of CO to singlet $[Ru(PH_3)_4]$ allowing for linear (C_{2v}) and non-linear (C_s) approaches of CO (LDA + NL)

respectively) shows that addition of CO to the model species is a strongly thermodynamically favoured process.

An *ab initio* study of addition of CO to Vaska's compound has found a transition state featuring a non-linear Ir–C–O unit to be more stable than its linear equivalent.[19a] Reaction profiles for the addition of CO to $[M(PH_3)_4]$ species, defined by the M–C distance, were therefore computed in both C_{2v} and C_s symmetry, the latter allowing the CO moiety to move off the local C_2 axis of the $[M(PH_3)_4]$ fragment if it was energetically favourable to do so. The computed reaction profiles are shown in Fig. 10 for M = Ru. Similar results were obtained for M = Fe. The addition of CO to $[M(PH_3)_4]$ species is computed to proceed without an activation barrier for both M = Fe and Ru once the non-linear approach of CO is taken into account. These results are consistent with the experimental rate constant obtained for the addition of CO to $[M(dmpe)_2]$ species which exceeded 10^9 dm^3 mol^{-1} s^{-1} for both metals and, in the case of Ru, was near diffusion control (*i.e.* very little, if any, activation energy).[6] At long M–C separations (>2.5 Å) we found that geometries with M–C–O angles of approximately 107° were favoured for both metals. Imposing a linear approach of CO (C_{2v} symmetry) resulted in a small activation barrier (≈2 kcal mol^{-1}) for both metals at long M–C separations (M–C > 3.5 Å).

Discussion

Structure and ground-state electronic configuration of $[M(dmpe)_2]$ species

The UV/VIS spectrum of $[Ru(dmpe)_2]$ suggests that this species has a geometry which is square planar or close to it.[7] The rate constants for reaction with CO and H_2 are close to the diffusion limit suggesting that $[Ru(dmpe)_2]$ has a singlet electronic state. The calculations on $[Ru(PH_3)_4]$ show that a near square-planar D_{2d} geometry with a singlet-state configuration is 11 kcal mol^{-1} more stable than the triplet configuration (C_{2v} geometry). The calculated energy of the $d_{z^2} > p_z$ transition is also consistent with the experimental results and the computed profiles for reaction with both H_2 and CO do not feature any activation barrier. Thus both experiment and calculation are in agreement with a near square-planar, singlet ground state for $[Ru(dmpe)_2]$.

For the iron system neither experiments nor calculations are so clear. Experimentally, the lack of correspondence in spectra and the different rates of reaction relative to the ruthenium system point to a change in structure. The reaction with CO is extremely rapid, but not close enough to the diffusion limit to exclude a triplet configuration. The experimental evidence for the role of specific solvation is inconclusive. The calculations on $[Fe(PH_3)_4]$ show that a C_{2v} triplet is more stable than a C_{2v} singlet structure by 8.0 kcal mol^{-1}. The $d_{z^2} \longrightarrow p_z$ transition of singlet $[Fe(PH_3)_4]$ is predicted to occur in the visible/near-IR

region of the spectrum, but no absorptions are observed within this spectral range. The calculations predict a small barrier for the addition of H_2 to singlet $[Fe(PH_3)_4]$ but no barrier for addition of CO. Overall the reactivity of singlet $[Fe(PH_3)_4]$ is predicted to be similar to that of singlet $[Ru(PH_3)_4]$. The experimental and theoretical evidence both argue therefore against a square-planar singlet ground state. Since the reaction may involve singlet $[Fe(dmpe)_2]$, triplet $[Fe(dmpe)_2]$ and the solvent adduct $[Fe(dmpe)_2S]$, calculations including this solvated species would therefore be necessary for a full understanding of the reactivity of the iron system. If one assumes a triplet structure for $[Fe(dmpe)_2]$ the activation energies for addition of CO and oxidative addition of H_2 can be estimated from the difference in energy between the triplet and singlet states to increase by 8.0 kcal mol^{-1}.

Influence of the L group on the singlet and triplet states of ML_4

The energy patterns computed for singlet and triplet $[M(PH_3)_4]$ are similar to those calculated previously for analogous $[M(CO)_4]$ species (M = Ru or Fe).[15] The geometries calculated here for singlet $[Fe(PH_3)_4]$ and triplet $[M(PH_3)_4]$ are also similar to their carbonyl analogues. However, our calculations predict a D_{2d} structure for singlet $[Ru(PH_3)_4]$ with angles of about 160° at Ru whereas singlet $[Ru(CO)_4]$ was computed to have a C_{2v} geometry with angles of about 175 and 130° at the metal. The mixed-ligand species $[Ru(CO)_2(PH_3)_2]$, appears to be closer to the tetracarbonyl complex since it adopts a singlet ground state with C–Ru–C and P–Ru–P angles of 133 and 173° respectively (MP2 optimisation).[9] These structural trends in the ruthenium systems are consistent with the conclusions of Elian and Hoffmann,[14] who showed that the tendency for d^8 ML_4 systems to deviate from square-planar geometry is associated with the presence of π-acceptor ligands and is consistent with the relatively weak π-acceptor capability of phosphine ligands.

Distortion away from a square-planar geometry is also a reflection of the metal centre. The C_{2v} structure of $[Ru(CO)_2(PH_3)_2]$ is promoted by strong π-back donation from the high-lying metal-based orbitals. In contrast, $[Rh(CO)_2(PH_3)_2]^+$, in which the metal-based orbitals are much lower in energy, adopts a square-planar geometry.[9] The deviations from square planarity calculated for singlet $[Fe(PH_3)_4]$ and $[Ru(PH_3)_4]$ in the present study suggest that π-back donation from high-lying metal-based orbitals is important in these systems with low-oxidation-state metal centres as well. The near square-planar structure computed for $[Rh(PH_3)_4]^+$ is consistent with these ideas.

Reactivity of singlet $[M(PH_3)_4]$ species

Oxidative addition of H_2. The oxidative addition of H_2 to $[M(PH_3)_4]$ species has been studied for three metal systems where M = Fe, Ru or Rh^+. Experimental data demonstrate that the iron and ruthenium experimental analogues, $[Fe(dmpe)_2]$ and $[Ru(dmpe)_2]$, are highly reactive species. In contrast, $[Rh(dmpe)_2]^+$ is unreactive enough to be characterised crystallographically. Starting from a singlet geometry, product formation is calculated to be strongly favoured thermodynamically with the iron and ruthenium model complexes. In contrast, addition of H_2 to $[Rh(PH_3)_4]^+$ is much less exothermic. We attempt to account for the greater reactivity of the neutral $[M(PH_3)_4]$ systems by employing an energy-decomposition scheme[50] to analyse the bonding between the $[M(PH_3)_4]$ and $\{H\cdots H\}$ fragments within $[Rh(PH_3)_4H_2]^+$ and $[Ru(PH_3)_4H_2]$. The major interactions between these two fragments are summarised in Fig. 11 in which the orbital numbering employed in the following discussion is also indicated.

The decomposition approach allows the bonding energy between two closed-shell fragments to be split up into a steric-repulsion term (ΔE^{steric}) and an orbital-interaction term (ΔE^{oi}); ΔE^{steric} is made up of the four-electron destabilising interactions between occupied orbitals (exchange repulsion) and the electrostatic interaction between the nuclear and electronic distributions of the two fragments. The orbital-interaction term can be further divided into contributions from each symmetry representation. We also consider the energy required to distort each of the two isolated reactants to arrive at the geometries found in the optimised structure of the product (ΔE^{prep}). The results of the energy decomposition analysis are given in Table 1.

Table 1 Energy decomposition data (kcal mol^{-1}) for $[M(PH_3)_4H_2]$ (M = Ru or Rh^+)

	$[Ru(PH_3)_4]$–$\{H\cdots H\}$	$[Rh(PH_3)_4]^+$–$\{H\cdots H\}$
ΔE^{steric}		
Exchange repulsion	206.3	240.2
Electrostatic	−208.2	−223.3
Total	−2.0	16.9
ΔE^{oi}		
a_1	−48.2	−59.7
b_2	−119.4	−113.1
Total	−168.1	−173.3
Total bonding energy	−170.1	−156.4
ΔE^{prep} *	14.2 + 115.0	25.3 + 112.5
ΔE^{form}	−37.6	−15.6

* The two figures refer to ΔE^{prep} terms for the $[M(PH_3)_4]$ and $\{H\cdots H\}$ fragments

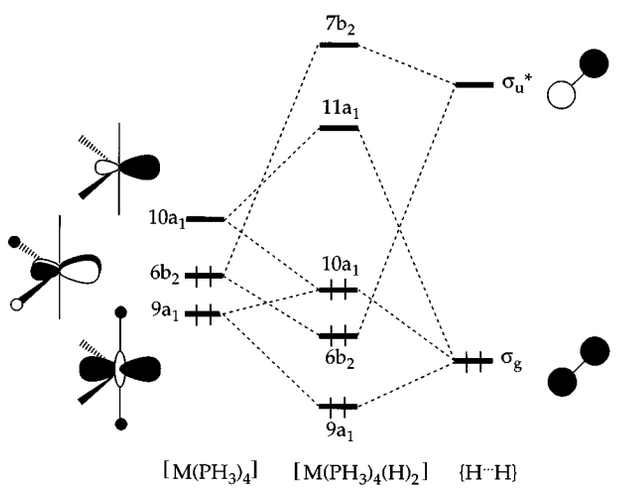

Fig. 11 Schematic representation of major interactions between $[M(PH_3)_4]$ and $\{H\cdots H\}$ fragments. The $3a_2$ and 6b, metal-based valence orbitals which are non-bonding with respect to the $\{H\cdots H\}$ fragment have been omitted for clarity

On comparing the ruthenium and Rh^+ systems, we find ΔE^{prep} to be 8.4 kcal mol^{-1} higher for $[Rh(PH_3)_4]^+$–$\{H\cdots H\}$, the majority of this difference resulting from the higher energy required to distort the $[Rh(PH_3)_4]^+$ moiety away from a square-planar geometry. Analysis of the ΔE^{steric} term indicates that the electrostatic interaction is more stabilising by 15 kcal mol^{-1} for $[Rh(PH_3)_4]^+$–$\{H\cdots H\}$, as would be expected for a cationic fragment. In contrast, the exchange repulsion term is less destabilising for $[Ru(PH_3)_4]$–$\{H\cdots H\}$ by 34 kcal mol^{-1}. Finally the orbital interaction contribution is larger for $[Rh(PH_3)_4]^+$–$\{H\cdots H\}$ by 5 kcal mol^{-1}. The major difference in ΔE^{form} therefore originates from ΔE^{steric} (19 kcal mol^{-1}) and can be traced to the much larger exchange repulsion seen in the Rh^+ system.

The origin of the larger exchange repulsion calculated in $[Rh(PH_3)_4H_2]^+$ compared with $[Ru(PH_3)_4H_2]$ must arise from

Table 2 Orbital populations (e) for the {H···H} fragment in $[M(PH_3)_4H_2]$ species (M = Ru or Rh^+)

M	Ru	Rh^+
σ_g	1.34	1.15
σ_u*	1.03	0.91

the interaction of the occupied σ_g orbital of {H···H} with occupied metal fragment orbitals of a_1 symmetry, in particular the metal-based $9a_1$ orbital. In general, one would expect the metal-based orbitals of a ruthenium(0) species to lie to much higher energy than those of an isoelectronic Rh^+ cation.[9] This should result in a larger energy gap between σ_g {H···H} and the $9a_1$ orbital of the ruthenium fragment, leading to reduced exchange repulsion in that case.

Although ΔE^{oi} between the $[M(PH_3)_4]$ and {H···H} fragments in the final product molecules is rather similar for both ruthenium and Rh^+ systems the contributions from the different symmetry representations depend on the nature of the metal centre. Thus for $[Ru(PH_3)_4]$–{H···H} we find the a_1 and b_2 orbital interactions contribute −48 and −119 kcal mol^{-1} respectively. The corresponding figures for $[Rh(PH_3)_4]^+$–{H···H} are −60 and −113 kcal mol^{-1}. These differences can again be understood in terms of the higher energy of the metal-based orbitals of the $[Ru(PH_3)_4]$ fragment. The high energy of the $6b_2$ orbital of $[Ru(PH_3)_4]$ should result in it acting as a better donor into σ_u*{H···H} than the equivalent low-lying $6b_2$ orbital of the $[Rh(PH_3)_4]^+$ fragment. For similar reasons the acceptor capabilities of the $10a_1$ orbital will be relatively poor in $[Ru(PH_3)_4]$ compared to $[Rh(PH_3)_4]^+$. These conclusions are supported by the calculated orbital populations of the σ_g and σ_u* orbitals of the {H···H} fragment in the final $[M(PH_3)_4H_2]$ species (see Table 2). The stronger acceptor nature of $[Rh(PH_3)_4]^+$ results in the more efficient depopulation of the σ_g orbital in this case while back donation into σ_u* is greater for $[Ru(PH_3)_4]$. However, in terms of the overall orbital interaction these two effects approximately cancel out.

A similar comparison between the iron and ruthenium systems is hampered by the different geometries of the species involved. This results in large changes in ΔE^{prep} and ΔE^{steric} which may simply reflect these geometrical changes rather than any difference in the intrinsic electronic properties of the iron and ruthenium centres. We shall therefore not use this fragmentation approach for the comparison of the first- and second-row transition-metal species.

Reaction with CO. The reactions of $[M(PH_3)_4]$ with CO (M = Fe or Ru) are both computed to be highly exothermic, consistent with the high reactivity of their $M(dmpe)_2$ experimental analogues. In this case ΔE^{form} can be equated to a M–CO bond dissociation enthalpy, ΔH, and is computed to be slightly larger for the iron system. This conclusion, that $\Delta H_{3d} > \Delta H_{4d}$, is consistent with the results of previous *theoretical*[15,51] determinations of M–CO bond dissociation in related polycarbonyl systems, including a recent study employing high-level *ab initio* calculations.[52] However, an *experimental* study of the first M–CO bond-dissociation enthalpy in Group 6 $M(CO)_6$ species gave the order $\Delta H_{5d} > \Delta H_{4d} > \Delta H_{3d}$.[53] We shall not pursue this issue further in the present paper but note that ΔE^{form} for the oxidative addition of H_2 to $[Fe(PH_3)_4]$ and $[Ru(PH_3)_4]$ is again computed to be larger for the first-row metal. For reasons discussed in the previous section we do not attempt a more detailed comparison of the 3d and 4d $M(PH_3)_4(CO)$ systems.

Reaction profiles. The different reaction profiles computed for the oxidative-addition reaction of H_2 to $[M(PH_3)_4]$ species allow us to propose the likely course of these reactions. For $[Ru(PH_3)_4]$ both the initial η^1 approach of H_2 and subsequent η^1/η^2 swing can occur without any activation barrier. For singlet $[Fe(PH_3)_4]$ both the η^1 and η^2 approaches appear equally probable, both requiring small activation energies (≈1 kcal mol^{-1}) at long Fe–x separations (>3.0 Å). The η^1/η^2 swing is again barrierless in this case. For $[Rh(PH_3)_4]^+$ the η^1 approach is favoured at long Rh–x separations, but we estimate the activation energy required for the η^1/η^2 swing to be at least comparable and possibly slightly larger than that estimated for the η^2 approach. The transition state in this case may well have a 'product-like' C_{2v} geometry with Rh–x ≈ 2.3 Å.

The different reaction profiles can be understood in terms of the fragmentation analysis performed above. For example, the absence of a barrier for the reaction between $[Ru(PH_3)_4]$ and H_2 is a result of the donor/acceptor characteristics of the metal species. The linear approach of H_2 is stabilised by good donation from the high-lying $9a_1$ into σ_u*(H_2) while any $9a_1/\sigma_g$ destabilisation is relatively small due to the large energy mismatch between these orbitals. This reduced destabilisation coupled with the strong π-donor power of the metal $6b_2$ orbital, which is further enhanced by the distortion of the $[Ru(PH_3)_4]$ moiety,[18–20] allows the reorientation and cleavage of the H_2 moiety to proceed without any activation barrier. The similar form of the reaction profile calculated between $[Fe(PH_3)_4]$ and H_2 suggests a comparable series of orbital interactions with decreasing Fe–x distances, although in this case we calculate a small activation barrier for the η^1 approach at Fe–x ≈ 3.5Å. This may simply be due to reduced overlap arising from the more contracted Fe-based orbitals in this case. The small activation barrier calculated for the reaction between singlet $[Fe(PH_3)_4]$ and H_2 may contribute to the slower reaction rate observed with $[Fe(dmpe)_2]$ compared to $[Ru(dmpe)_2]$. However, as the precise nature of the transient species formed in the case of the iron complex is not known, the role played by this activation barrier in determining the overall reaction rate is not clear. As for $[Fe(CO)_4] + H_2$,[45] the triplet ground state of $[Fe(PH_3)_4]$ complicates any analysis of reaction profiles.

For the reaction of $[Rh(PH_3)_4]^+$ with H_2 the linear approach is again preferred at long Rh–x separations. However, reorientation of the H_2 moiety entails a significant activation barrier due to the low energy of the metal $9a_1$ orbital (greater $9a_1/\sigma_g$ destabilisation) and the lower π-donor ability of the metal $6b_2$ orbital in this case. Overall an η^2 approach may be favoured in this case as this maximises the donation from σ_g (H_2) into the low-lying $10a_1$ acceptor orbital of the $[Rh(PH_3)_4]^+$ fragment.

Similar considerations apply to the addition of CO to $[M(PH_3)_4]$ species (M = Fe or Ru). In this case the four-electron destabilisation occurs between the lone pair of CO and the $9a_1$ metal-based orbital. However, as has been described previously for the addition of CO to *trans*-$[Ir(PH_3)_2(CO)Cl]$,[19a] this destabilisation can be reduced by a non-linear approach of CO towards the metal fragment. The early stages of this reaction have been described as a nucleophilic attack of the metal-based a_1 HOMO on the π* acceptor orbital of CO.

For the addition of CO to $[M(PH_3)_4]$ species the computed reaction curves indicate that the non-linear approach of CO can completely override the effect of any four-electron destabilisation early in the reaction profile. The subsequent reaction then proceeds without any activation barrier. This is in contrast to the above study of the reactivity of Vaska's complex where an activation barrier of 4.6 kcal mol^{-1} was calculated. This difference is again probably a reflection of the high energy of the metal-based orbital in our systems which results in better M→CO π donation and reduced four-electron destabilisation compared to the equivalent interactions involving *trans*-$[Ir(PH_3)_2(CO)Cl]$.

Conclusion

Density functional calculations have been carried out on

$[M(PH_3)_4]$ as models for transient $[M(dmpe)_2]$ species which are formed from the photolysis of $[M(dmpe)_2H_2]$ (M = Fe or Ru). Calculations have also been performed on $[Rh(PH_3)_4]^+$ as a model for the relatively inert $[Rh(dmpe)_2]^+$.

The singlet electron configurations of $[Ru(PH_3)_4]$ and $[Rh(PH_3)_4]^+$ were found to have D_{2d} geometries with *trans*–P–M–P angles of 159 and 172° respectively. Singlet $[Fe(PH_3)_4]$ was computed to have a C_{2v} structure with angles of 137 and 160° at Fe. The structure of $[Ru(PH_3)_4]$ differs, therefore, from the isoelectronic $[Ru(CO)_4]$ and $[Ru(CO)_2L_2]$ species while the computed structure of singlet $[Fe(PH_3)_4]$ is similar to that calculated for singlet $[Fe(CO)_4]$. The triplet configurations of $[Fe(PH_3)_4]$ and $[Ru(PH_3)_4]$ were predicted to adopt C_{2v} geometries with P–M–P angles *ca*. 155 and 95° and thus resemble analogous $[M(CO)_4]$ triplet species (M = Fe or Ru). For $[Ru(PH_3)_4]$ the singlet structure is calculated to be 11 kcal mol^{-1} more stable than the triplet, while the triplet form of $[Fe(PH_3)_4]$ is 8 kcal mol^{-1} more stable in this case. The singlet/triplet energetic preferences have therefore now been calculated for the two known pairs of homoleptic ML_4 species (M = Fe or Ru, L = CO or PH_3).

The calculations on $[Ru(PH_3)_4]$ and $[Rh(PH_3)_4]^+$ reproduce the UV/VIS spectra, geometries and relative reactivities of these species towards H_2 satisfactorily. For $[Ru(PH_3)_4]$ the reaction with H_2 is calculated to be highly exothermic and to proceed without an activation barrier. For $[Rh(PH_3)_4]^+$ the reaction with H_2 is much less thermodynamically favoured and proceeds with an activation barrier of approximately 3 kcal mol^{-1}. The reaction between H_2 and singlet $[Fe(PH_3)_4]$ is also highly exothermic and proceeds with a small activation barrier at long Fe–H_2 separations. An η^1 approach of H_2 to $[M(PH_3)_4]$ (M = Fe or Ru) is preferred at large M···H_2 separations, but H_2 is predicted to tilt to an η^2 orientation in the later stages of reaction. Elongation of the H···H distance occurs very late in the reaction profile. Although the η^1 approach is computed to be more stable at long Rh^+···H_2 separations, the transition state formed with $[Rh(PH_3)_4]^+$ is likely to have an η^2-H_2 geometry.

The addition of CO to $[M(PH_3)_4]$ (M = Fe or Ru) is calculated to be highly exothermic. With an angled approach of CO, the activation energy for reaction with both species is zero.

The zero {or, in the case of singlet $[Fe(PH_3)_4] + H_2$, minimal} activation energies computed for the reactions of $[M(PH_3)_4]$ species (M = Fe or Ru) with H_2 and CO reflect the high energies of the metal-based valence orbitals of these systems. This allows the metal centre to act as a strong electron donor and reduces the four-electron destabilisation that occurs upon approach of the substrate molecule. The high energy of the metal-based valence orbitals results in these species being relatively poor acceptors of electron density. However, any acceptor capabilities will be enhanced by a small HOMO–LUMO gap and will further promote low activation barriers.

Acknowledgements

We thank the EPSRC for a Western European NATO Fellowship (S. A. M.) and support (R. N. P., M. K. W.). The Laboratoire de Chimie Théorique is associated with the Centre National de la Recherche Scientifique (URA 506) and is a member of Institut de Chimie Moléculaire d'Orsay and Institut de Physico-Chimie Moléculaire. S. A. M. also thanks the EU Human Capital and Mobility Network (CHRX CT 93 0152) for a travel grant and Professor E. J. Baerends and his group for useful discussions. We thank Dr. A. J. Downs for providing facilities for measuring the NIR spectrum of $[Fe(dmpe)_2]$.

References

1 R. Hoffmann, *Angew. Chem., Int. Ed. Engl.*, 1982, **21**, 711.
2 M. Poliakoff, *Chem. Soc. Rev.*, 1978, **7**, 527.
3 M. Poliakoff and E. Weitz, *Acc. Chem. Res.*, 1987, **20**, 408; R. J. Ryther and E. Weitz, *J. Phys. Chem.*, 1991, **95**, 9841; W. Wang, A. A. Narducci, P. G. House and E. Weitz, *J. Am. Chem. Soc.*, 1996, **118**, 8654.
4 F. W. Grevels, in *Photoprocesses in Transition-metal Complexes, Biosystems and Other Molecules. Experiment and Theory*, ed. E. Kochansky, Kluwer, Dordrecht, 1992.
5 P. L. Bogdan and E. Weitz, *J. Am. Chem. Soc.*, 1989, **111**, 3163.
6 M. K. Whittlesey, R. J. Mawby, R. Osman, R. N. Perutz, L. D. Field, M. P. Wilkinson and M. W. George, *J. Am. Chem. Soc.*, 1993, **115**, 8627.
7 C. Hall, W. D. Jones, R. J. Mawby, R. Osman, R. N. Perutz and M. K. Whittlesey, *J. Am. Chem. Soc.* , 1992, **114**, 7425.
8 B. Yau and L. D. Field, personal communication.
9 M. Ogasawara, S. A. Macgregor, W. E. Streib, K. Folting, O. Eisenstein and K. G. Caulton, *J. Am. Chem. Soc.*, 1995, **117**, 8869; 1996, **118**, 10 189.
10 R. J. Mawby, R. N. Perutz and M. K. Whittlesey, *Organometallics*, 1995, **14**, 3268.
11 L. D. Field, A. W. George and B. A. Messerle, *J. Chem. Soc., Chem. Commun.*, 1991, 1339.
12 J. K. Burdett, *J. Chem. Soc.*, *Faraday Trans. 2*, 1974, 1599.
13 J. K. Burdett, *Inorg. Chem.*, 1975, **14**, 375.
14 M. Elian and R. Hoffmann, *Inorg. Chem.*, 1975, **14**, 1058.
15 (*a*) T. Ziegler, V. Tschinke, L. Fan and A. D. Becke, *J. Am. Chem. Soc.*, 1989, **111**, 9177; (*b*) T. Ziegler, *Inorg. Chem.*, 1986, **25**, 2721; (*c*) J. Li, G. Schreckenbach and T. Ziegler, *J. Am. Chem. Soc.*, 1995, **117**, 486.
16 (*a*) W. Wang and E. Weitz, *J. Phys. Chem. A.*, 1997, **101**, 2358; (*b*) E. Ruiz, P. Alemany, S. Alvarez and J. Cano, *J. Am. Chem. Soc.*, 1997, **119**, 1297.
17 P. E. M. Siegbahn, M. R. A. Blomberg and M. Svensson, *J. Am. Chem. Soc.*, 1993, **115**, 4191; P. E. M. Siegbahn and M. R. A. Blomberg, *Organometallics*, 1994, **13**, 354; P. E. M. Siegbahn, *Organometallics,* 1994, **13**, 2833.
18 J. O. Noell and P. J. Hay, *J. Am. Chem. Soc.*, 1982, **104**, 4578; J.-Y. Saillard and R. Hoffmann, *J. Am. Chem. Soc.*, 1984, **106**, 2006.
19 (*a*) F. Abu-Hasanayn, K. Krogh-Jesperson and A. S. Goldman, *J. Am. Chem. Soc.*, 1994, **116**, 5979; (*b*) F. Abu-Hasanayn, K. Krogh-Jesperson and A. S. Goldman, *Inorg. Chem.*, 1993, **32**, 495; (*c*) F. Abu-Hasanayn, A. S. Goldman and K. Krogh-Jesperson, *J. Phys. Chem.*, 1993, **97**, 5890.
20 A. Sevin, *Nouv. J. Chim.*, 1981, **5**, 233.
21 A. Dedieu and A. Strich, *Inorg. Chem.*, 1979, **18**, 2940.
22 F. M. Bickelhaupt, E. J. Baerends and W. Ravenek, *Inorg. Chem.*, 1990, **29**, 350.
23 T. R. Cundari, *J. Am. Chem. Soc.*, 1994, **116**, 340.
24 N. Koga and K. Morokuma, *J. Phys. Chem.*, 1990, **94**, 5454; *Chem. Rev.*, 1991, **91**, 823; F. Maseras, N. Koga and K. Morokuma, *Organometallics*, 1994, **13**, 4008; S. Obara, K. Kitaura and K. Morokuma, *J. Am. Chem. Soc.*, 1984, **106**, 7482; D. G. Musaev and K. Morokuma, *J. Am. Chem. Soc.*, 1995, **117**, 799; N. Koga and K. Morokuma, *J. Am. Chem. Soc.*, 1993, **115**, 6883.
25 A. L. Sargent and M. B. Hall, *Inorg. Chem.*, 1992, **31**, 317; A. L. Sargent, M. B. Hall and M. F. Guest, *J. Am. Chem. Soc.*, 1992, **114**, 517; J. Song and M. B. Hall, *Organometallics*, 1993, **12**, 3118.
26 Y. Jean and A. Lledos, *Nouv. J. Chim.*, 1986, **10**, 635.
27 S. Sakaki and Y. Musashi, *J. Chem. Soc., Dalton Trans.*, 1994, 3047.
28 R. H. Crabtree, *Angew. Chem., Int. Ed. Engl.*, 1993, **32**, 789; C. Hall and R. N. Perutz, *Chem. Rev.*, 1996, **96**, 3125.
29 R. G. Parr and W. Yang, *Density Functional Theory of Atoms and Molecules*, Oxford University Press, New York, 1989; E. S. Kryachko and E. V. Ludena, *Density Functional Theory of Many Electron Systems*, Kluwer, Dordrecht, 1990; V. Tschinke and T. Ziegler, *Can. J. Chem.*, 1989, **67**, 460.
30 T. Ziegler, *Chem. Rev.*, 1991, **91**, 651; L. Fan and T. Ziegler, *J. Chem. Phys.,* 1991, **95**, 7401.
31 T. B. Marder and I. D. Williams, *J. Chem. Soc.*, *Chem. Commun.*, 1987, 1478.
32 R. A. Jones, F. M. Real, G. Wilkinson, A. M. R. Galas, M. B. Hursthouse and K. M. A. Malik, *J. Chem Soc.*, *Dalton Trans.*, 1980, 511.
33 R. R. Schrock and J. A. Osborn, *J. Am. Chem. Soc.*, 1971, **93**, 2397.
34 E. J. Baerends, D. E. Ellis and P. Ros, *Chem. Phys.*, 1973, **2**, 71; E. J. Baerends, J. G. Snijders, C. A. de Lange and G. Jonkers, in *Local Density Approximations in Quantum Chemistry and Solid State Physics*, eds. J. P. Dahl and J. Avery, Plenum, New York, 1984.
35 G. te Velde and E. J. Baerends, *J. Comput. Phys.*, 1992, **99**, 84.
36 J. G. Snijders, E. J. Baerends and P. Vernooijs, *At. Data Nucl. Data Tables*, 1982, **26**, 483; P. Vernooijs, J. G. Snijders and E. J. Baerends, *Slater type basis functions for the whole periodic system*, Internal Report, Free University of Amsterdam, 1981.

37 T. Ziegler, V. Tschinke, E. J. Baerends, J. G. Snijders and W. Ravenek, *J. Chem. Phys.*, 1989, **93**, 3050.
38 S. J. Vosko, L. Wilk and M. Nusair, *Can. J. Phys.*, 1980, **58**, 1200.
39 L. Versluis and T. Ziegler, *J. Chem. Phys.*, 1988, **88**, 322.
40 A. D. Becke, *Phys. Rev. A.*, 1988, **38**, 3098.
41 J. P. Perdew, *Phys. Rev. B.*, 1986, **33**, 8822.
42 W. D. Jones and E. Libertini, *Inorg. Chem.*, 1986, **25**, 1794.
43 A. G. Orpen, L. Brammer, F. H. Allen, O. Kennard, D. G. Watson and R. Taylor, *J. Chem Soc.*, *Dalton Trans.*, 1989, S1.
44 T. A. Albright, J. K. Burdett and M.-H. Whangbo, *Orbital Interactions in Chemistry*, Wiley, New York, 1985.
45 J. S. Ricci, T. F. Koetzle, M. T. Bautista, T. M. Hofstede, R. H. Morris and J. F. Sawyer, *J. Am. Chem. Soc.*, 1989, **111**, 8823.
46 L. S. Van Der Sluys, J. Eckert, O. Eisenstein, J. H. Hall, J. C. Huffmann, S. A. Jackson, T. F. Koetzle, G. J. Kubas, P. J. Vergamini and K. G. Caulton, *J. Am. Chem. Soc.*, 1990, **112**, 4831.
47 M.-J. Fernandez, P. M. Bailey, P. O. Bentz, J. S. Ricci, T. F. Koetzle and P. M. Maitlis, *J. Am. Chem. Soc.*, 1984, **106**, 5458.
48 L. Brammer, W. T. Klooster and F. R. Lemke, *Organometallics*, 1996, **15**, 1721.
49 F. A. Cotton, K. I. Hardcastle and G. A. Rusholme, *J. Coord. Chem.*,1973, **2**, 217.
50 T. Ziegler, *NATO ASI Ser. C.*, 1992, **378**, 367.
51 T. Ziegler, V. Tschinke and C. Ursenbach, *J. Am. Chem. Soc.*, 1987, **109**, 4825.
52 A. W. Ehlers, S. Dapprich, S. F. Vyboishchikov and G. Frenking, *Organometallics*, 1996, **15**, 105.
53 K. E. Lewis, D. M. Golden and G. P. Smith, *J. Am. Chem. Soc.*, 1984, **106**, 3905.

Received 19*th August* 1997; *Paper* 7/06081E